VOL. 18, NO. 17, SEPTEMBER 2023 ISSN 1819-6608
ARPN Journal of Engineering and Applied Sciences

www.arpnjournals.com

LATERAL TORSIONAL BUCKLING OF UNSYMMETRIC BEAMS BY FEM WITH LINEAR ELEMENTS

Nazzal S. Armouti
Department of Civil Engineering, University of Jordan, Amman, Jordan
E-Mail: armouti@ju.edu.jo

ABSTRACT

As the exact solution of lateral torsional buckling of elastic prismatic beams is practically limited to the simple case of simply supported beams under equal end moments, other loading conditions and boundary conditions require more practical solutions to the problem. As the general solution of lateral torsional buckling of unsymmetric beams is a function of the sign of the bending moment along the axis of the beam, i.e. location of the shear center concerning the compression zone of the cross section, application of the current traditional empirical expressions such as coefficient of the moment, C_b, becomes highly inconsistent and unwarranted to capture the correct critical moment as acknowledged by the American Institute of Steel Construction, AISC. The finite element method, FEM, offers a feasible alternative to overcome these shortcomings. FEM is formulated in its simplest form of linear elements for the general case of lateral torsional buckling of unsymmetric cross sections. Finite element development shows that the characteristic equation is of the nonlinear quadratic eigenvalue problem type. Using the classical polynomial shape functions for beams, FEM proves to be extremely accurate and can overcome the high inconsistencies and discrepancies embedded in the application of the classical methods.

Keywords: finite element method, lateral torsional buckling of unsymmetric beams.

Manuscript Received 6 July 2023; Revised 19 October 2023; Published 8 November 2023

INTRODUCTION

Lateral torsional buckling of beams is one of the cumbersome problems that face engineers. In general, lateral torsional buckling can be classified into two categories, first, beams with sections symmetric about their major axis and at the same time bent about this major axis, and second, unsymmetric beams or monosymmetic beams about their minor axis and bent about their major axis; the other axis of symmetry (Galambus, 1968).

Due to the length of treatment of both categories, symmetric and asymmetric, the first class of beams, i.e. symmetric beams, were treated in a previous paper (Armouti, 2022). This paper will address the second class of beams, i.e. unsymmetric beams

Many analytical and experimental studies have been conducted to tackle the problem of lateral torsional buckling, LTB, of unsymmetric beams. LTB of unsymmetric beams is considered a 3D problem and is usually treated with the 3D finite element method, FEM, using shell elements. Other analytical methods exist, such as energy and numerical methods, however, they are considered cumbersome and not suited for practical applications. For example, (Hauksoon, 2014) explored some of the popular commercial software programs he discussed their advantages, shortcomings, and limitations especially when it comes to unsymmetric cross sections. (Piotrowski, 2015) studied LTB of monosymmetric I-beams with warping restraint at supports using energy methods, and then compared with the results of 3D volumetric elements. (Asgarian, 2011) studied LTB of non-prismatic unsymmetric I-beams using the total potential energy method, and then compared the results with 3D shell elements. 3D shell elements are also used to study the LTB of T-beams with opening (Ahmad, 2021). In addition, experimental and numerical analysis are used to study the LTB of monosymmetric and unsymmetric sections (Bajer *et al*. 2017), and experimental and numerical analysis are also used to study the LTB of beams with selected cross-sections (Barnat *et al*. 2017).

The exact solution of the lateral torsional buckling problem exists for the simple case of the simply supported beam under an equal end moment. Other support conditions and loading schemes are treated mainly by empirical methods. Over the years, the American Institute of Steel Construction (AISC) (AISC, 2017) provided empirical equations and some coefficient of moment to treat some selected cases. However, in Sec. F12 of its commentary, the AISC code calls for more practical and realistic methods to treat the general case of lateral torsional buckling of unsymmetric beams. Within this context, the finite element method offers an attractive and practical solution to this problem.

The differential equation of lateral torsional buckling for unsymmetric beams is obtained by second-order analysis (Galambus, 1968), which is given in the following form

$$EC_w\phi^{iv} - \{GJ + M_{o\beta}\beta_x\}\phi'' - \frac{M_{o\beta}^2}{EI_y}\phi = 0$$

where

E = Young modulus.
G = Shear modulus.
C_w = Warping constant, also known as warping moment of inertia, (m^6).
J = Saint Venant torsional constant, (m^4).

I_y = Moment of inertial of the cross-section about the weak axis, y, (m^4).

β_x = Coefficient of monosymmetry of the cross-section which reflects its unsymmetry as will be defined in the following paragraphs, (m).

$M_{o\beta}$ = Externally applied equal end moment in the presence of, β_x, as shown in Figure-1.

ϕ = Twisting angle of the cross section about the z-axis as shown in Figure-1, (rad)

ϕ'', ϕ^{iv} = Second and four derivative of, ϕ, with respect to the axis, z.

z = Centroidal axis

Within this context, bracing conditions will be identified as follows:

- **Simple brace:** a brace that provides restriction of the rotation angle, but permits warping at the section under consideration, i.e. $\phi = 0$, $\phi' \neq 0$.
- **Fixed brace:** a brace that provides restriction for both rotation and warping of the section under consideration, i.e. $\phi = 0$, $\phi' = 0$.

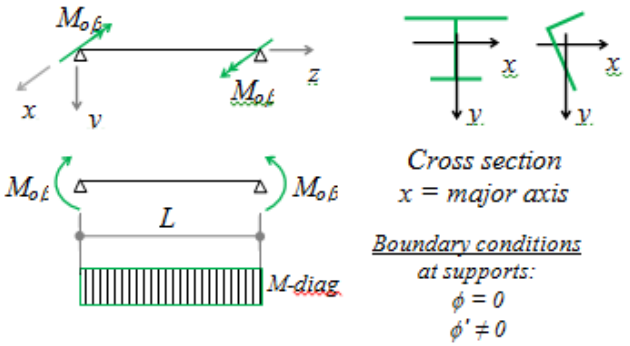

Figure-1. Simply supported beam under equal end moments, free to warp, and braced against rotation at supports.

The exact solution for the case of the simply supported beam under equal end moments, free to warp, and laterally braced against rotation at the supports, as shown in Figure 1, is given in the following form (Galambus, 1968)

$$M_{o\beta cr} = \left(\frac{\pi}{\ell}\right)^2 EI_y \left\{ \frac{\beta_x}{2} \pm \sqrt{\left(\frac{\beta_x}{2}\right)^2 + \left(\frac{GJ}{\left(\frac{\pi}{\ell}\right)^2 EI_y} + \frac{EC_w}{EI_y} \right)} \right\}$$

where, $\beta_x = \left(\frac{\int y\,(x^2 + y^2)\,dA}{I_x} - 2y_s \right)$

x, y = Major and minor principal axes.

y_s = y-coordinate of the shear center concerning the principal axes, x, and y.

with the following sign convention

β_x = +ve when the shear center lies in the compression zone of the cross section.

β_x = -ve when the shear center lies in the tension zone of the cross section.

It is worth mentioning that the above expression includes two unequal solutions which can be shown that the results depend on the sign of, β_x. If the critical moment of symmetric sections is considered a reference, i.e. β_x, is taken zero, then the unsymmetric section solution will be higher than, M_{ocr}, when, β_x, is positive; and will be lower than, M_{ocr}, when, β_x, is negative. In other words, the lateral torsion buckling of unsymmetric beams depends on the direction of the moment concerning the location of the shear center, whereas it is independent of the direction of the moment in the case of symmetric cross sections.

FINITE ELEMENT FORMULATION

To obtain the finite element solution of this problem, the Galerkin method of finite element formulation, which operates directly on the differential equation, offers an attractive approach to accomplish this task (Huebner and Thornton). A quick review of the Galerkin Method reminds us that an approximate function of the solution (shape functions) can be assumed, and then minimization of the error by weighted residuals yields the required results. It is well documented that the weighted residuals in the Galerkin method are taken as the shape functions themselves.

Accordingly, for the differential equation presented earlier, the twisting angle, $\phi(z)$, may be approximated as, $\bar{\phi}(z)$, which can be expressed in terms of shape functions as follows

$$\bar{\phi}(z) = \sum_j \psi_j(z)\,\phi_j$$

where

$\bar{\phi}(z)$ = approximate continuous function of field twisting angle.

$\psi_j(z)$ = continuous shape function of field twisting angle, ϕ.

ϕ_j = nodal twisting angle.

If a function, $f(z)$, is defined such as

$$f(z) = EC_w\phi^{iv} - (GJ + M_{o\beta}\,\beta_x)\,\phi'' - \frac{M_{o\beta}^2}{EI_y}\phi = 0$$

And if the approximate function, $\bar{\phi}(z)$, is used instead of the exact function, $\phi(z)$, then, $f(z)$, becomes an approximate function, which does not vanish but yields a residual value, or an error due to the approximation, i.e.

$$\bar{f}(z) = EC_w\bar{\phi}^{iv} - (GJ + M_{o\beta}\,\beta_x)\,\bar{\phi}'' - \frac{M_{o\beta}^2}{EI_y}\bar{\phi} \neq 0 =$$

residual value

Consequently, there will be an error in the solution equal to the difference between the approximate and exact solution, i.e.

$$\text{error} = \bar{f}(z) - f(z) = \bar{f}(z) - 0 = \bar{f}(z)$$

The weighted residuals method states that the summation of the error components multiplied by their weights is set to zero. Galerkin contribution to this method was to consider the weights to be the shape functions themselves, hence, the integrated weighted residuals become

$$\int \text{error} \cdot \text{weight} \cdot dz = 0$$

$$\text{or, } \int \left(EC_w \bar{\phi}^{iv} - (GJ + M_{o\beta}\beta_x)\bar{\phi}'' - \frac{M_{o\beta}^2}{EI_y}\bar{\phi} \right) \cdot \psi_i \, dz = 0$$

Substitution of, $\bar{\phi}(z) = \sum_j \psi_j(z)\phi_j$, in the above expression yields

$$\sum_j \int \left(EC_w \psi_j^{iv}\phi_j - GJ\,\psi_j''\phi_j - M_{o\beta}\beta_x\psi_j''\phi_j - \frac{M_{o\beta}^2}{EI_y}\psi_j\phi_j \right) \cdot \psi_i \, dz = 0$$

$$\text{or, } \sum_j \int \left(EC_w \psi_j^{iv}\psi_i\phi_j - GJ\,\psi_j''\psi_i\phi_j - M_{o\beta}\beta_x\psi_j''\psi_i\phi_j - \frac{M_{o\beta}^2}{EI_y}\psi_j\psi_i\phi_j \right) \cdot dz = 0$$

By integration by parts, the above integrals can be converted into symmetric integrals which yields the following expression

$$\sum_j \int \left(EC_w \psi_i''\psi_j''\phi_j + GJ\,\psi_i'\psi_j'\phi_j + M_{o\beta}\beta_x\psi_i'\psi_j'\phi_j - \frac{M_{o\beta}^2}{EI_y}\psi_i\psi_j\phi_j \right) \cdot dz = 0 \quad \ldots \quad i = 1, 2, 3, 4$$

Note that the highest derivative in the integrals above is a second derivative, and hence, the shape functions must maintain continuity at the nodes up to the first derivative, i.e. ϕ'. Consequently, the beam needs four Degrees Of Freedom (DOFs) to satisfy this continuity requirement, namely, the twisting angle and its first derivative at each node of the beam. Note also that these four DOFs require four shape functions. For beams, the popular four polynomial shape functions shown in Figure-2 are ideal for this development.

The integration of the expression given above yields the corresponding 4x4 element matrices which may be identified and given within this context as follows:

1. Element warping stiffness matrix, $[C_{we}]$, where $C_{we\,ij} = \int EC_w \psi_i''\psi_j'' \, dz$

$$\text{or, } [C_{we}] = \frac{EC_w}{L^3}\begin{bmatrix} 12 & 6L & -12 & 6L \\ 6L & 4L^2 & -6L & 2L^2 \\ -12 & -6L & 12 & -6L \\ 6L & 2L^2 & -6L & 4L^2 \end{bmatrix}$$

$$\psi_1 = +1 - 3\left(\frac{x}{L}\right)^2 + 2\left(\frac{x}{L}\right)^3$$

$$\psi_2 = +x\left(1 - \frac{x}{L}\right)^2$$

$$\psi_3 = +3\left(\frac{x}{L}\right)^2 - 2\left(\frac{x}{L}\right)^3$$

$$\psi_4 = -\left(\frac{x^2}{L}\right)\left(1 - \frac{x}{L}\right)$$

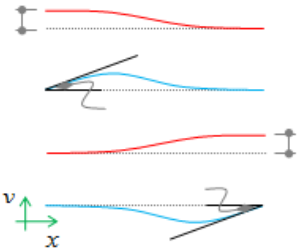

Figure-2. Popular polynomial shape functions used for beam formulation.

2. Element Saint Venant stiffness matrix, $[J_e]$, where $J_{e\,ij} = \int GJ\,\psi_i'\psi_j' \, dz$

$$\text{or, } [J_e] = \frac{GJ}{30L}\begin{bmatrix} 36 & 3L & -36 & 3L \\ 3L & 4L^2 & -3L & -L^2 \\ -36 & -3L & 36 & -3L \\ 3L & -L^2 & -3L & 4L^2 \end{bmatrix}$$

3. Element coefficient of monosymmetry matrix, $[\beta_{xe}]$, where $\beta_{xe\,ij} = \int \beta_x\,\psi_i'\psi_j' \, dz$

$$\text{or, } [\beta_{xe}] = \frac{\beta_x}{30L}\begin{bmatrix} 36 & 3L & -36 & 3L \\ 3L & 4L^2 & -3L & -L^2 \\ -36 & -3L & 36 & -3L \\ 3L & -L^2 & -3L & 4L^2 \end{bmatrix}$$

4. Element lateral stiffness matrix, $[I_y]$, where $I_{y\,ij} = \int \frac{1}{EI_y}\psi_i\psi_j \, dz$

$$\text{or, } [I_{ye}] = \frac{L}{420\,EI_y}\begin{bmatrix} 156 & 22L & 54 & -13L \\ 22L & 4L^2 & 13L & -3L^2 \\ 54 & 13L & 156 & -22L \\ -13L & -3L^2 & -22L & 4L^2 \end{bmatrix}$$

As pointed out earlier, continuity requirements result in four nodal DOFs with 2DOFs at each end. Figure-3 shows the resulting arrangement of these local (element) DOFs as related to the above element matrices. In this paper, the rotation angle will be represented by a curve with a single arrow head whereas the curvature is represented by a curve with double arrow heads as shown in Figure-3. Using the vector {U} to represent the local (element) DOFs, the {U} vector appears as follows

$$\{U\} = \begin{Bmatrix} u_1 \\ u_2 \\ u_3 \\ u_4 \end{Bmatrix}, \text{ which correspondent to, } \{\phi\}_{\text{element}} = \begin{Bmatrix} \phi_i \\ \phi_i' \\ \phi_j \\ \phi_j' \end{Bmatrix},$$

as shown in Figure-3.

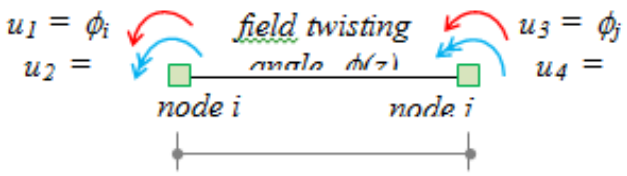

Figure-3. Definition of element Degrees of Freedom of beams in terms of twisting angle, ϕ.

Accordingly, the element local matrices take the form

$[C_{we}]\{U\}$, $[J_e]\{U\}$, $[\beta_{xe}]\{U\}$, $[I_{ye}]\{U\}$

Recall that curvature is defined as the rate of change of rotation concerning length, and hence, ϕ', may be viewed as the twisting curvature which is resulting from the effect of warping integral in this case. Note that this twisting curvature appears in this formulation as a new and additional DOF to the beam which becomes the so-called the seventh DOF of the beam modeling the effect of warping in the section.

Given the above, and after constructing the counterpart global matrices by a standard assembly process, the finite element formulation may be symbolically presented in a matrix form. Using the vector {D} to represent the global DOFs, and for several DOFs equal to, N, the final matrix formulation is given as follows

$$[C_w]\{D\} + [J]\{D\} + M_{o\beta}[\beta_x]\{D\} - M_{o\beta}^2[I_y]\{D\} = \{0\}$$

or, $$\{[C_w] + [J] + M_{o\beta}[\beta_x] - M_{o\beta}^2[I_y]\}\{D\} = \{0\}$$

or, $$\{[[C_w] + [J]] + M_{o\beta}[\beta_x] - M_{o\beta}^2[I_y]\}\{D\} = \{0\}$$

where

$[C_w]$ = Global warping stiffness matrix size NxN.
$[J]$ = Global Saint Venant stiffness matrix size NxN.
$[\beta_x]$ = Global coefficient of monosymmetry matrix size NxN.
$[I_y]$ = Global lateral torsional geometric stiffness matrix size NxN.
$M_{o\beta}$ = Lateral torsional moments with numbers equal to N.
$\{D\}$ = Global nodal vector size Nx1 as defined previously.
$= \{d_1\ d_2\ d_3\ \dots\ d_N\}^T$

The resulting equation above is a quadratic eigenvalue problem which might be presented in the following form

$$\{[K] + \lambda[C] - \lambda^2[M]\}\{\phi\} = \{0\}$$

The above lateral torsional buckling matrices represent a set of homogeneous linear algebraic equations with a size equal to N and hence represent the characteristic equation of the lateral torsional buckling moments. Note that, unlike the case of symmetric cross sections which yields a generalized eigenvalue problem, the unsymmetric cross section case yields a nonlinear quadratic eigenvalue problem form.

Note that the quadratic eigenvalue problem is different from the standard eigenvalue problem as it contains two expressions of the unknown eigenvalue, λ, raised to the first power and to the second power as shown. Accordingly, the standard eigenvalue solution cannot be used in this case and hence the solution may be obtained by other methods (Tisseur and Meerbergen, 2001). In this paper, successive iteration procedures are implemented to find each of the eigenvalues that make the resulting determinant value equal to zero, and then the correspondent eigenvector is obtained by solving the resulting system of linear algebraic equations for a selected relative value for one element of the eigenvector column (chosen to be, 1, for element No. 1, as will be shown later). Such a solution yields an, N, lateral torsional buckling moment and an, N, corresponding mode shape.

FINITE ELEMENT APPLICATION AND VERIFICATION

The application procedures and verification of this method will be demonstrated by considering the beam shown in Figure-4. Using middle line dimensions, the relevant section properties are calculated as shown in Table-1.

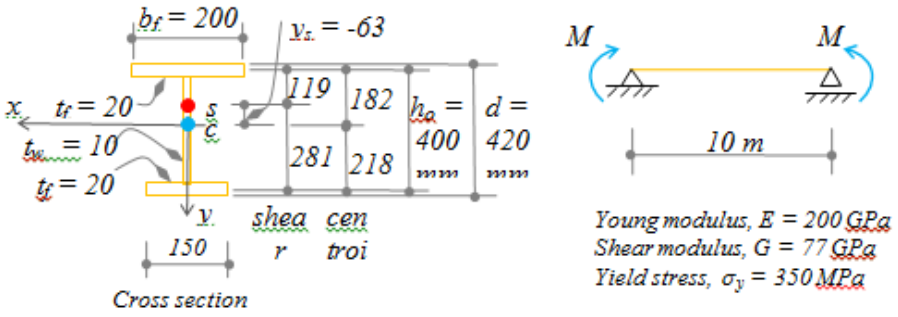

Figure-4. I-beam layout and boundary conditions, simple supports with simple braces, i.e. $\phi = 0$, $\phi' \neq 0$.

Table-1. I-beam section properties calculations.

	Equation expression	Arithmetic detail	Section property value	Stiffness value
Flanges moment of inertia, I_f	$I_{f1} = \frac{t_{f1}\, b_{f1}^3}{12}$	$\frac{20\,(200)^3}{12}$	13.333×10^6	-----
	$I_{f2} = \frac{t_{f2}\, b_{f2}^3}{12}$	$\frac{20\,(150)^3}{12}$	5.625×10^6	-----
Warping constant, C_w	$h_o^2 \frac{I_{f1}\, I_{f2}}{I_{f1} + I_{f2}}$	$(400)^2 \frac{13.333\ (5.625)}{13.333 + 5.625} \times 10^6$	$C_w = 632.962 \times 10^9$ mm^6	$EC_w = 126.592$ kN.m^4
Torsional Constant, J	$\sum \frac{b\,t^3}{3}$	$\frac{200\,(20)^3}{3} + \frac{150\,(20)^3}{3} + \frac{400\,(10)^3}{3}$	$J = 1.067 \times 10^6$ mm^4	$GJ = 82.133$ kN.m^2
Coefficient of monosymmetry, β_x	By integration	See text body for details *	153 mm (0.153 m)	-----
Transverse moment of inertia, I_y	ΣI_{fi}	$13.333 \times 10^6 + 5.625 \times 10^6$	$I_y = 18.958 \times 10^6$ mm^4	$EI_y = 3,791.667$ kN.m^2

*β_x $= \left(\frac{\int y\,(x^2 + y^2)\,dA}{I_x} - 2y_s \right)$. As β_x calculations are rather cumbersome, the intermediate results are given here concerning Figure 4 as follows:

y_s = y-coordinate of the shear center which may be obtained by classical procedures of shear center calculations to yield, $y_s = -63.137$ mm.

I_x = the moment of inertial of the entire cross section about the major, x-axis, which may be obtained by standard procedures to yield, $I_x = 329,696,970$ mm^4.

The integration above may be carried over the three components of the cross section separately, namely, top flange, web, and bottom flange to yield the following result,

Top flange → $\int y\,x^2\,dA = -2.424 \times 10^9$, $\int y^3\,dA = -24.042 \times 10^9$

Web → $\int y\,x^2\,dA = 0$, $\int y^3\,dA = 2.933 \times 10^9$

Bottom flange → $\int y\,x^2\,dA = 1.227 \times 10^9$, $\int y^3\,dA = 31.160 \times 10^9$

Knowing the above quantities, β_x, can now be calculated as follows:

$$\beta_x = \left(\frac{\int y\,(x^2 + y^2)\,dA}{I_x} - 2y_s \right) = 153 \text{ mm.}$$

Recall that the sign of, β_x, depends on the location of the shear center concerning the compression zone which is taken positive if the shear center lies in the compression zone, and negative if the shear center lies in the tension zone of the cross section.

This beam is simply supported, simply braced, and subjected to equal end moments which put the shear center in the compression zone, hence, β_x, is taken equal to +0.153 m. The exact solution of this case is presented in the introduction; therefore, the exact critical lateral torsional moment in presence of the β_x-coefficient, $M_{o\beta+}$, is given as follows:

$$M_{o\beta\,cr} = \left(\frac{\pi}{\ell}\right)^2 EI_y \left\{ \frac{\beta_x}{2} \pm \sqrt{\left(\frac{\beta_x}{2}\right)^2 + \left(\frac{GJ}{\left(\frac{\pi}{\ell}\right)^2 EI_y} + \frac{EC_w}{EI_y} \right)} \right\}$$

$$M_{o\beta\,cr} = \left(\frac{\pi}{10}\right)^2 (3,791.667) \left\{ \frac{0.153}{2} \pm \sqrt{\left(\frac{0.153}{2}\right)^2 + \left(\frac{82.133}{\left(\frac{\pi}{10}\right)^2 (3,791.667)} + \frac{126.592}{3,791.667} \right)} \right\}$$

$$= \begin{pmatrix} +218.973 \\ -161.717 \end{pmatrix} \text{ kN.m}$$

Note that the solution yields two answers, a positive moment which puts the shear center in the compression zone, and a negative moment which puts the shear center in the tension zone. It should be pointed out that if the coefficient of monosymmetry, β_x, is taken negative, an inspection of the above expression indicates that the answers will be (+161.717 and -218.973) which means that the answer will be the same with switched signs. This conclusion indicates that the correct critical moment depends on the location of the shear center concerning the compression zone in the section. This result also indicates that the higher critical moment takes place when the shear center lies in the compression zone, whereas the smaller critical moment takes place when the shear center lies in the tension zone.

In this paper, and for clarity of presentation, the critical buckling moment for the standard case of equal end moments applied to a simply supported beam with a uniform cross section will be referred to by the following designation according to the presence of shear center concerning the compression zone

$M_{o\beta+cr}$ = Critical buckling moment when, β_x is positive, i.e. shear center in the compression zone.

$M_{o\beta-cr}$ = Critical buckling moment when, β_x is negative, i.e. shear center in the tension zone.

$M_{o\beta cr}$ = Critical buckling moment regardless of the sign of, β_x, whether positive or negative.

The FEM solution is obtained by standard procedures. In this section, a demonstration of the procedures will be presented using two identical elements as shown in Figure-5. Since the supports provide a simple brace, i.e. $\phi = 0$, $\phi' \neq 0$, the beam will have four global DOFs, namely, two twisting curvatures at the supports, i.e. at Nodes 1 and 2, and one rotation, one twisting curvature at midspan, i.e. at Node 2 as shown in Figure-5.

The procedures of application will include the solution of both cases of coefficient of monosymmetry, β_x, i.e. a case of positive, β_x, and a case of negative, β_x, as follows:

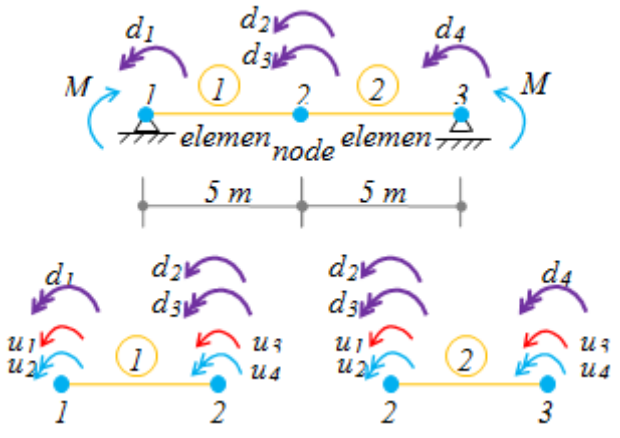

Figure-5. Beam discretization into two equal elements.

Case 1: β_x = +153 mm:

Element matrices:

Note that since the two elements are identical, the element matrices will be the same for both of them. Using kN, and m units, the matrices are calculated as follows:

$$[C_{we1}] = [C_{we2}] = [C_{we}] = \frac{EC_w}{L^3}\begin{bmatrix} 12 & 6L & -12 & 6L \\ 6L & 4L^2 & -6L & 2L^2 \\ -12 & -6L & 12 & -6L \\ 6L & 2L^2 & -6L & 4L^2 \end{bmatrix} =$$

$$\begin{bmatrix} 12.153 & 30.383 & -12.153 & 30.383 \\ 30.383 & 101.275 & -30.383 & 50.638 \\ -12.153 & -30.383 & 12.153 & -30.383 \\ 30.383 & 50.638 & -30.383 & 101.275 \end{bmatrix}$$

$$[J_{e1}] = [J_{e2}] = [J_e] = \frac{GJ}{30L}\begin{bmatrix} 36 & 3L & -36 & 3L \\ 3L & 4L^2 & -3L & -L^2 \\ -36 & -3L & 36 & -3L \\ 3L & -L^2 & -3L & 4L^2 \end{bmatrix} =$$

$$\begin{bmatrix} 19.712 & 8.213 & -19.712 & 8.213 \\ 8.213 & 54.755 & -8.213 & -13.689 \\ -19.712 & -8.213 & 19.712 & -8.213 \\ 8.213 & -13.689 & -8.213 & 54.755 \end{bmatrix}$$

$$[\beta_{xe1}] = [\beta_{xe\,2}] = [\beta_{xe}] = \frac{\beta_x}{30L}\begin{bmatrix} 36 & 3L & -36 & 3L \\ 3L & 4L^2 & -3L & -L^2 \\ -36 & -3L & 36 & -3L \\ 3L & -L^2 & -3L & 4L^2 \end{bmatrix} =$$

$$\begin{bmatrix} 0.037 & 0.015 & -0.037 & 0.015 \\ 0.015 & 0.102 & -0.015 & -0.026 \\ -0.037 & -0.015 & 0.037 & -0.015 \\ 0.015 & -0.026 & -0.015 & 0.102 \end{bmatrix}$$

$$[I_{ye1}] = [I_{ye2}] =$$

$$[I_{ye}] = \frac{L}{420\,EI_y}\begin{bmatrix} 156 & 22L & 54 & -13L \\ 22L & 4L^2 & 13L & -3L^2 \\ 54 & 13L & 156 & -22L \\ -13L & -3L^2 & -22L & 4L^2 \end{bmatrix} =$$

$$10^{-6}\begin{bmatrix} 490 & 345 & 170 & -204 \\ 345 & 314 & 204 & -235 \\ 170 & 204 & 490 & -345 \\ -204 & -235 & -345 & 314 \end{bmatrix}$$

Assembly of the global matrices, $[K_g]$, in terms of the global 4DOFs, d_1, d_2, d_3, d_4, can be carried out from

the element matrices, $[k_e]$, using the following expression (Chen and Lui, 1987)

$[K_g] = \Sigma\, [T]^T\, [k_e]\, [T]$… summation is carried out over all elements

where, [T], is known as the kinematic (compatibility) matrix which relates the global nodal deformations {D} to element nodal deformations {U}. Accordingly, the [T] matrices for elements, 1 and 2, are constructed as follows:

$$[T_1]^T = \begin{array}{c} \\ d_1 \\ d_2 \\ d_3 \\ d_4 \end{array} \begin{array}{c} \begin{array}{cccc} u_1 & u_2 & u_3 & u_4 \end{array} \\ \begin{bmatrix} 0 & 1 & 0 & 0 \\ 0 & 0 & 1 & 0 \\ 0 & 0 & 0 & 1 \\ 0 & 0 & 0 & 0 \end{bmatrix} \end{array}, \quad [T_2]^T = \begin{array}{c} \\ d_1 \\ d_2 \\ d_3 \\ d_4 \end{array} \begin{array}{c} \begin{array}{cccc} u_1 & u_2 & u_3 & u_4 \end{array} \\ \begin{bmatrix} 0 & 0 & 0 & 0 \\ 1 & 0 & 0 & 0 \\ 0 & 1 & 0 & 0 \\ 0 & 0 & 0 & 1 \end{bmatrix} \end{array}$$

Carrying out the above summation leads to

$$[C_w]_{\text{global}} = \Sigma\, [T_i]^T\, [C_{we,i}]\, [T_i] = \begin{bmatrix} 101.275 & -30.383 & 50.638 & 0 \\ -30.383 & 24.306 & 0 & 30.383 \\ 50.638 & 0 & 202.550 & 50.638 \\ 0 & 30.383 & 50.638 & 101.275 \end{bmatrix}$$

$$[J]_{\text{global}} = \Sigma\, [T_i]^T\, [J_{,i}]\, [T_i] = \begin{bmatrix} 54.755 & -8.213 & -13.689 & 0 \\ -8.213 & 39.424 & 0 & 8.213 \\ -13.689 & 0 & 109.511 & -13.689 \\ 0 & 8.213 & -13.689 & 54.755 \end{bmatrix}$$

$$[\beta_x]_{\text{global}} = \Sigma\, [T_i]^T\, [\beta_{x,i}]\, [T_i] = \begin{bmatrix} 0.102 & -0.015 & -0.026 & 0 \\ -0.015 & 0.073 & 0 & 0.015 \\ -0.026 & 0 & 0.204 & -0.026 \\ 0 & 0.015 & -0.026 & 0.102 \end{bmatrix}$$

$$[I_y]_{\text{global}} = \Sigma\, [T_i]^T\, [I_{y,i}]\, [T_i] = 10^{-6} \begin{bmatrix} 314 & 204 & -235 & 0 \\ 204 & 980 & 0 & -204 \\ -235 & 0 & 628 & -235 \\ 0 & -204 & -235 & 314 \end{bmatrix}$$

Characteristic equation:

$$\{\, [\, [C_w] + [J]\,] + M_{o\beta+}\, [\beta_x] - M_{o\beta+}{}^2\, [I_y]\, \}\, \{D\} = \{0\}$$

$$\left\{ \begin{bmatrix} 156.031 & -38.596 & 36.949 & 0 \\ -38.596 & 63.730 & 0 & 38.596 \\ 36.949 & 0 & 312.061 & 36.949 \\ 0 & 38.596 & 36.949 & 156.031 \end{bmatrix} + M_{o\beta+} \begin{bmatrix} 0.102 & -0.015 & -0.026 & 0 \\ -0.015 & 0.073 & 0 & 0.015 \\ -0.026 & 0 & 0.204 & -0.026 \\ 0 & 0.015 & -0.026 & 0.102 \end{bmatrix} \right.$$

$$\left. - M_{o\beta+}{}^2\, 10^{-6} \begin{bmatrix} 314 & 204 & -235 & 0 \\ 204 & 980 & 0 & -204 \\ -235 & 0 & 628 & -235 \\ 0 & -204 & -235 & 314 \end{bmatrix} \right\} \begin{Bmatrix} d_1 \\ d_2 \\ d_3 \\ d_4 \end{Bmatrix} = \begin{Bmatrix} 0 \\ 0 \\ 0 \\ 0 \end{Bmatrix}$$

The solution of the above quadratic eigenvalue equation is obtained by successive iterations which yields four moments, { $M_{o\beta+}$ }, and four mode shapes, [ϕ], as follows:

$$\{M_{o\beta+}\} = \begin{Bmatrix} 219.108 \\ 596 \\ 1,248 \\ 2,129 \end{Bmatrix}, [\,\phi\,] = \left[\phi_1 \;\vdots\; \phi_2 \;\vdots\; \phi_3 \;\vdots\; \phi_4\right] = \left[\begin{array}{c:c:c:c} 1 & 1 & 1 & 1 \\ 3.167 & 0 & -0.548 & 0 \\ 0 & -1 & 0 & 1 \\ -1 & 1 & -1 & 1 \end{array}\right]$$

Graphical presentation of the mode shapes are also shown in Figure-6 (a and b). The critical lateral torsional buckling moment is, of course, the smallest of the four moments which is given as follows:

$M_{o\beta+cr}$ = 219.108 kN.m … vs … exact = 218.973 kN.m

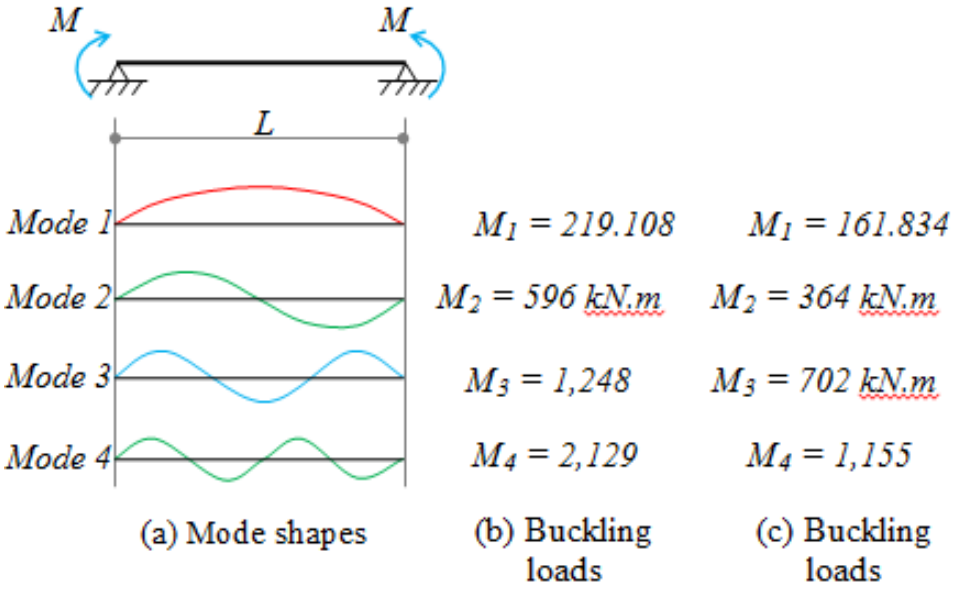

Figure-6. Buckling moments and their mode shapes.

As well-known and documented, the accuracy of the FEM solution depends on the size of the mesh (number of elements) in this case. To examine the effect of the mesh size on the accuracy of this solution, the above procedures are repeated for, 1, 2, 3, 5, and 10 elements. The results are summarized in Table-2.

Table-2. Critical lateral torsional buckling moment for various FEM mesh sizes β_x = positive = + 0.153 m.

	Exact solution	**Number of elements**				
		1	**2**	**3**	**5**	**10**
Critical moment, $M_{o\beta+cr}$ kN.m	218.973	223.283	219.108	218.997	218.976	218.973
% error	0 %	1.97 %	0.06 %	0.01 %	0.001 %	≅ 0 %

Table-2 shows that the accuracy of the solution is very accurate and almost exact if, 10, elements are used. It can also be seen that using one element which is considered crude mesh, the error is still around 2%. For all practical purposes, it can be seen that three elements are more than enough to get very accurate results. However, in the general case where the moment gradient is not constant but rather varies along the axis of the section, several elements should be selected to capture the effect of variation of the moment gradient in what is known as the sensitivity analysis in FEM.

Case 2: β_x = - 153 mm:

The FEM solution of this case results in identical matrices as in the case of positive, β_x, except for the matrix, $[\beta_x]$, which will be the negative sign of Case 1, i.e.

$$[\beta_x]_{global} = \Sigma\, [T_i]^T\, [\beta_{x,i}]\, [T_i] =$$

$$\begin{bmatrix} -0.102 & 0.015 & 0.026 & 0 \\ 0.015 & -0.073 & 0 & -0.015 \\ 0.026 & 0 & -0.204 & 0.026 \\ 0 & -0.015 & 0.026 & -0.102 \end{bmatrix}$$

Consequently, the characteristic equation becomes:

$$\{\, [\, [C_w] + [J]\,] + M_{o\beta-}\, [\beta_x] - M_{o\beta-}{}^2\, [I_y]\, \}\, \{D\} = \{0\}$$

$$\left\{ \begin{bmatrix} 156.031 & -38.596 & 36.949 & 0 \\ -38.596 & 63.730 & 0 & 38.596 \\ 36.949 & 0 & 312.061 & 36.949 \\ 0 & 38.596 & 36.949 & 156.031 \end{bmatrix} + M_{o\beta-} \right.$$
$$\left. \begin{bmatrix} -0.102 & 0.015 & 0.026 & 0 \\ 0.015 & -0.073 & 0 & -0.015 \\ 0.026 & 0 & -0.204 & 0.026 \\ 0 & -0.015 & 0.026 & -0.102 \end{bmatrix} \right\}$$
$$- M_{o\beta-}{}^2\, 10^{-6} \begin{bmatrix} 314 & 204 & -235 & 0 \\ 204 & 980 & 0 & -204 \\ -235 & 0 & 628 & -235 \\ 0 & -204 & -235 & 314 \end{bmatrix} \begin{Bmatrix} d_1 \\ d_2 \\ d_3 \\ d_4 \end{Bmatrix} = \begin{Bmatrix} 0 \\ 0 \\ 0 \\ 0 \end{Bmatrix}$$

The solution of the above quadratic eigenvalue equation is obtained by successive iterations which yields four moments, $\{ M_{o\beta-} \}$, and four mode shapes, $[\phi]$, as follows

$$\{M_{o\beta-}\} = \begin{Bmatrix} 161.834 \\ 364 \\ 702 \\ 1{,}155 \end{Bmatrix}, [\phi] = \left[\phi_1 \;\vdots\; \phi_2 \;\vdots\; \phi_3 \;\vdots\; \phi_4\right] =$$
$$\left[\begin{array}{c:c:c:c} 1 & 1 & 1 & 1 \\ 3.167 & 0 & -0.545 & 0 \\ 0 & -1 & 0 & 1 \\ -1 & 1 & -1 & 1 \end{array}\right]$$

Graphical presentation of the mode shapes is also shown in Figure 6 (a and c). The critical lateral torsional buckling moment is, of course, the smallest of the four moments which is given as follows

$M_{o\beta-cr}$ = 161.834 kN.m … vs … exact = 161.717 kN.m

Similar to Case 1, and to examine the effect of the mesh size on the accuracy of this solution, the above procedures are repeated for, 1, 2, 3, 5, and 10 elements. The results are summarized in Table-3.

Table-3. Critical lateral torsional buckling moment for various FEM mesh sizes β_x = negative = - 0.153 m.

	Exact solution	Number of elements				
		1	2	3	5	10
Critical moment, $M_{o\beta-cr}$ kN.m	161.717	165.271	161.834	161.739	161.720	161.717
% error	0 %	2.20 %	0.07 %	0.01 %	0.002 %	≅ 0 %

Table-3 shows that the accuracy of the solution is very much similar to Case 1, and hence might be treated similarly.

It is worth pointing out that as the coefficient of monosymmetry, β_x, gets smaller, the two critical positive and negative moments approach each other until they coincide at, $\beta_x = 0$. It can be shown that the critical moment of symmetrical sections at zero, β_x, is not the average of both critical moments in the case of unsymmetrical sections.

THE GENERAL CASE AND COMPARISON WITH AISC PROVISIONS

Similar to the case of symmetric sections, AISC treats the general case of lateral torsional buckling with the help of the well-known concept of equivalent moment coefficient, C_b. In this approach, the critical moment of the basic case of the simply supported beam under equal end moment, $M_{o\beta cr}$, is calculated and then multiplied by the coefficient, C_b, to account for the difference in the end moment, and later, was revised to account for the moment gradient between the bracing points. Accordingly, the critical moment, M_{cr}, is then calculated as

$$M_{cr} = C_b\, M_{o\beta cr}$$

As can be interpreted from the above expression, the coefficient, $C_b = M_{cr} / M_{o\beta cr}$, may be viewed as an indicator for the critical moment in the beam which will be used later for comparison between various cases.

In the past decade, AISC considered an empirical expression for, C_b that considers moment gradient which is developed by Kirby and Nethercot (Kirby and Nethercot, 1979). ASIC used a slightly modified and more conservative form of Kirby and Nethercot expression which is given in its modified form as follows:

$$C_b = \frac{12.5\, M_{max}}{2.5\, M_{max} + 3\, M_A + 4\, M_B + 3\, M_C}$$

where

M_{max} = absolute maximum moment between bracing points.

M_A = absolute moment at one quarter point between bracing points.

M_B = absolute moment at the midpoint between bracing points.

M_C = absolute moment at three quarter points between bracing points.

The accuracy, or the conservatism, embedded in this empirical expression of the equivalent moment coefficient, C_b, in the case of symmetric sections, was examined for some popular cases (Armouti, 2022). While this approach was shown to work reasonably for symmetric cross sections, it may not be equally applicable in the case of unsymmetric sections as will be demonstrated later.

It is important, at this point, to remind the reader of the essential difference between the critical moment of monosymmetric and unsymmetric beams. While the critical moment of symmetric sections and monosymmetric sections about the major axis of the beam is independent of the moment direction in the beam, the critical moment of unsymmetric section and monosymmetric sections about the minor axis of the beam depends on the moment direction in the beam in addition to the distribution of the internal moment along the beam axis. This issue creates an inconsistency in the application of the coefficient, C_b, in the case of unsymmetric cross sections of beams.

It seems that this inconsistency in the application of the coefficient, C_b, in the case of unsymmetric beams is one of the reasons that make the code uneasy about using the traditional approach of, C_b, as a general procedure and calls for more realistic and practical methods in evaluating the critical buckling moment of unsymmetric beams.

In this paper, the objective will be to examine the treatment of AISC to lateral torsional buckling of some unsymmetric sections which is presented for individually selected shapes in the AISC manual. The three cases addressed by AISC will be examined in this paper and compared with the FEM solution, namely, Unequal flange monosymmetric I-beam loaded in its web plane, T-section loaded in its stem plane, and unequal leg angle bent about its major axis. As AISC treats these three cases differently and separately, they will be presented separately in the following sections.

For each cross section, four loading cases will be considered, a one-side moment, opposite end moments, a concentrated load in a fixed-ends beam, and a concentrated load in flexural fixation and with warping released restraint at supports as shown in Figure-7. It is worth mentioning that the third and fourth cases are introduced because the AISC code does not recognize the warping restraint in its expressions, and therefore, there will be no basis for comparison with fixed bracing. Therefore, the fourth case is selected to simulate a fixed-ends beam in flexure with released restraint for warping to make a comparison with AISC expression on one hand and to examine the effect of warping restraint on the critical moment on the other.

Unequal Flange I-Beams are Monosymmetric about the Web and Loaded in the Web Plane

To avoid repetition of calculations, the cross section presented in Figure-4 will be used for this analysis. Figure-7 shows the four selected cases where, C_b, is calculated for each case using the AISC expression. In addition, for each case, the critical moment is calculated using FEM for both cases of positive and negative coefficient of monosymmetry, β_x, and then divided by the standard critical moment, $M_{o\beta cr}$. In other words, the FEM coefficient of the moment, $C_{b,\ FEM}$, is evaluated. The results of the critical moments for these cases are presented in Table-4.

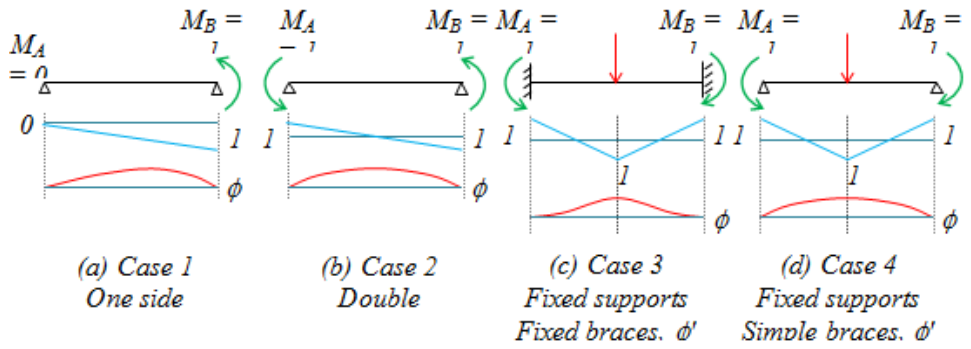

Figure-7. Selected cases of loading and support conditions with their applied moment diagrams and resulting mode shapes, ϕ-angle.

Table-4. Comparison between AISC empirical expression and FEM solution unequal flange I-beam.

Method of Analysis	Coefficient of Moment, C_b							
	Case 1*		Case 2*				Case 4*	
	C_b	$\frac{C_{b,AISC}}{C_{b,FEM}}$	C_b	$\frac{C_{b,AISC}}{C_{b,FEM}}$	C_b	$\frac{C_{b,AISC}}{C_{b,FEM}}$	C_b	$\frac{C_{b,AISC}}{C_{b,FEM}}$
AISC	1.67	---	2.27	---	1.92	---	1.92	---
FEM, β_x = + ve	1.82	0.92	2.08	1.09	1.84	1.04	1.36	1.41
FEM, β_x = - ve	1.78	0.94	2.82	0.81	2.55	0.75	2.18	0.88

*The four cases are shown in Figure-7.

T-Sections Loaded in Their Web Plane

The treatment of the T-section will be illustrated using the cross section shown in Figure-8. The span length and support conditions will remain the same as given in the case of unsymmetric I-section.

It is well documented that sections that are composed of a series of bars meeting at one point, such as T-sections, have a warping constant equal to zero, i.e. $C_w = 0$. The T-section properties can be obtained with a similar procedure of the I-beam case except for the C_w. The results are shown in Table-5.

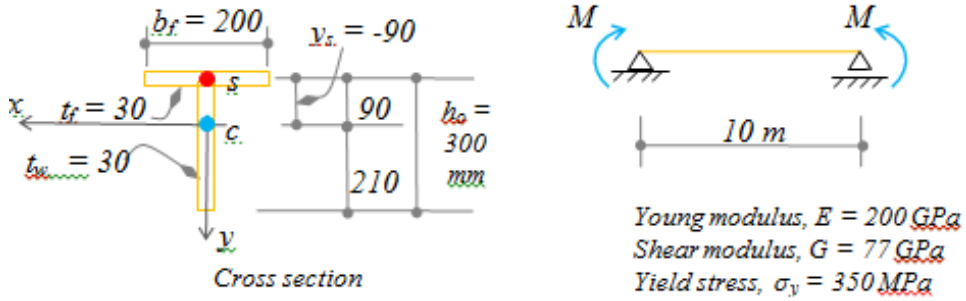

Figure-8. T-beam layout and boundary conditions, simple supports with simple braces, i.e. $\phi = 0$, $\phi' \neq 0$.

Table-5. T-beam section properties calculations.

J	GJ	I_y	EI_y	C_w	β_x
4.5 x10^6 mm^4	346.5 kN.m^2	20 x10^6 mm^4	4,000 kN.m^2	0	233 mm (0.233 m)

Using the values in Table-5, the theoretical exact critical load is given as follows:

$$M_{o\beta cr} = \begin{pmatrix} 418.696 \\ -326.711 \end{pmatrix} \text{kN.m}$$

Performing the same analysis presented in the I-beam case, the, C_b, values are obtained for both AISC and FEM as shown in Table-6.

Table-6. Comparison between AISC empirical expression and FEM solutionT-beam.

Method of Analysis	Coefficient of Moment, C_b							
	Case 1*		Case 2*		Case 3*		Case 4*	
	C_b	$\frac{C_{b,AISC}}{C_{b,FEM}}$	C_b	$\frac{C_{b,AISC}}{C_{b,FEM}}$	C_b	$\frac{C_{b,AISC}}{C_{b,FEM}}$	C_b	$\frac{C_{b,AISC}}{C_{b,FEM}}$

AISC	1.67	---	2.27	---	1.92	---	1.92	---
FEM, β_x = + ve	1.80	0.93	1.97	1.15	1.45	1.32	1.42	1.35
FEM, β_x = - ve	1.72	0.97	2.53	0.90	2.03	0.95	2.00	0.96

*The four cases are shown in Figure-7.

Unequal Leg Angles Bent About Their Major Axes

The treatment of the L-section will be illustrated using the cross section shown in Figure-9. The span length and support conditions will remain as given in the case of unsymmetric I-sections. Because the lateral torsional buckling analysis is based on the principal centroidal axes, the orientation and loading of the beam cross section must be applied in the plane of the principal minor axis, y, as shown in Figure-9.

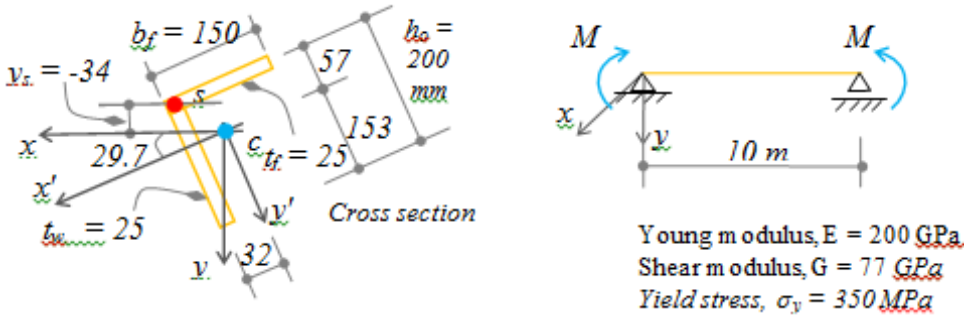

Figure-9. L-beam layout and boundary conditions, simple supports with simple braces, i.e. $\phi = 0$, $\phi' \neq 0$.

Consequently, and about Figure-9, the section properties can be obtained with a similar procedure of the I-beam case, using the principal axes, x, and y, and noting that $C_w = 0$. The results are presented in Table-7.

Table-7. L-beam section properties calculations.

J	GJ	I_y	EI_y	C_w	β_x
1.823 x10^6 m^4	140.365 N.m^2	9.918 x10^6 mm^4	1,983.6 kN.m^2	0	83 mm (0.083 m)

Using the values in Table-7, the theoretical exact critical load is given as follows:

$$M_{o\beta cr} = \begin{pmatrix} 176.875 \\ -160.626 \end{pmatrix} \text{kN.m}$$

The analysis of the L-section will be similar to the previous both cases of I-sec and T-sec. However, to make a comprehensive comparison, the coefficient of moment, C_b, is calculated twice. First, C_b, is calculated using the general expression by AISC with limits equal to, 3, i.e. $C_b \leq 3$, as shown in Table 8(a), and second, C_b, is calculated using the same expression by AISC with limits for angles equals to, 1.5, i.e. $C_b \leq 1.5$, as shown in Table 8(b).

Table-8(a). Comparison between AISC empirical expression and FEM solution L-beam ($C_b \leq 3$).

Method of Analysis	Coefficient of Moment, C_b							
	Case 1*		Case 2*		Case 3*		Case 4*	
	C_b	$\frac{C_{b,AISC}}{C_{b,FEM}}$	C_b	$\frac{C_{b,AISC}}{C_{b,FEM}}$	C_b	$\frac{C_{b,AISC}}{C_{b,FEM}}$	C_b	$\frac{C_{b,AISC}}{C_{b,FEM}}$

AISC	1.67	---	2.27	---	1.92	---	1.92	---
FEM, β_x = + ve	1.78	0.94	2.35	0.97	1.64	1.17	1.61	1.20
FEM, β_x = - ve	1.75	0.95	2.60	0.88	1.87	1.03	1.84	1.05

*The four cases are shown in Figure-7.

Table-8(b). Comparison between AISC empirical expression and FEM solution L- beam ($C_b \leq 1.5$).

Method of Analysis	**Coefficient of Moment, C_b**							
	Case 1*		**Case 2***		**Case 3***		**Case 4***	
	C_b	$\frac{C_{b,AISC}}{C_{b,FEM}}$	C_b	$\frac{C_{b,AISC}}{C_{b,FEM}}$	C_b	$\frac{C_{b,AISC}}{C_{b,FEM}}$	C_b	$\frac{C_{b,AISC}}{C_{b,FEM}}$
AISC	1.67	---	2.27	---	1.92	---	1.92	---
FEM, β_x = + ve	1.78	0.84	2.35	0.64	1.64	0.91	1.61	0.93
FEM, β_x = - ve	1.75	0.86	2.60	0.58	1.87	0.80	1.84	0.82

*The four cases are shown in Figure-7.

DISCUSSIONS

In this section, the results obtained and presented in the previous sections will be analyzed. Tables 4, 6, 8(a), and 8(b) are combined and presented in Figure 10 and Figure-11 for positive and negative values of, β_x, respectively. Note that a value of, C_b-ratio, above one in these figures indicates an overestimation of the critical moment by AISC expression, and hence the beam would be unsafe.

An important difference and variation between the cross section and load cases are highlighted to examine their effect on the analysis. First, note that the T and L sections have zero warping constants, i.e. no resistance to warping. Second the value of, β_x, for the T and L sections are 233 mm and 83 mm respectively, which means that the T-section value of, β_x, is almost three times its value of the L-section.

Figure-10 indicates that the AISC empirical expression results for, C_b, are not always conservative. It shows that the beam is safe (C_b-ratio $\leq$ 1) when the moment diagram lies on one side of the beam (Case 1), i.e. when the sign of, β_x, does not change along the axis of the beam. However, when the bending moment diagram starts to lie on both sides of the beam where, β_x, flips from positive to negative and visa versa, the values of, C_b-ratio, start to exceed one which indicates that AISC overestimates the critical moment, and hence the beam becomes unsafe. The reason for this discrepancy is that when the value of, β_x, is negative in some regions of the beam, it will reduce the critical moment in these portions. Examination of the AISC expression reveals that the AISC does not recognize these changes and does not consider them.

Consequently, it can be concluded that the validity of AISC, C_b, is dependent on the location and distribution of the internal bending moment diagram about the axis of the beam which creates regions of positive and negative coefficient of, β_x. Figure-10 shows clearly that the more variation of the sign and distribution of the internal moment, the more deviation of results in the value of, C_b-ratio, takes place i.e. going from less variation in Case 2 to more variation in Case 4. Furthermore, the AISC solution becomes unconservative when the moment starts to lie and vary on both sides of the beam as in Case 2 to Case 4. The situation becomes more distinct and even worse with larger variations of the moment. This fact is reflected in the AISC expression as it overestimates the critical load by 9% in Case 2 and by 41% in Case 4.

Figure-11 shows the opposite effect that appears in Figure-10 which means that AISC offers a conservative solution when β_x, is negative; and the internal moment appears only on one side of the beam as in Case 1. When the moment starts to lie and vary on both sides of the beam as in Case 2 to Case 4, the AISC solution becomes more conservative where the underestimation of the critical moment reaches up to 81% of the actual critical moment as shown in Case 2.

Figure-10 shows that applying the, C_b, concept to the case of positive, β_x, is disadvantageous and brings the C_b-ratio, above one because the variation of the bending moment diagram along the beam axis simply decreases the base critical moment, $M_{o\beta+cr}$, in regions when, β_x, becomes negative. This reduction in the base moment is not considered by AISC as it applies, C_b, to a base moment of constant value along the beam axis similar to the case of symmetric cross sections. On the other hand, Figure-11

shows exactly the opposite effect as variation of the moment diagram along the beam axis increases the base critical moment, $M_{o\beta-cr}$, in regions when, β_x, becomes positive.

The effect of warping restraint on the critical moment and its impact on AISC, C_b, expression can be examined by comparing Case 3 (warping restraint) with Case 4 (warping release) results which indicate that there is a significant drop in the critical moment of the I-beam (up to 40% in Figure-10) when warping restraint is released. However, the warping release has negligible effect on the other three cross sections, T, and L, because their warping constant equals zero, and therefore they do not have warping resistance. As pointed out earlier, the warping presence is not recognized by the AISC expression of, C_b.

The effect of, β_x, on the critical moment and its impact on AISC, C_b, expression can be examined by comparing Figures 10 and 11. To exclude the effect of warping in this case, consider the cross section of zero warping constants for comparison, i.e. T and L sections. The differences again appear in the cases of variation of sign and distribution of moment diagram along the beam axis (cases, 2, 3, and 4). It can be seen from Figures 10 and 11 that the higher the value of, β_x, the further the results between positive and negative, β_x, are pushed apart. Recall that the value, β_x, for T-section and L-section are, 233 mm and 83 mm, respectively.

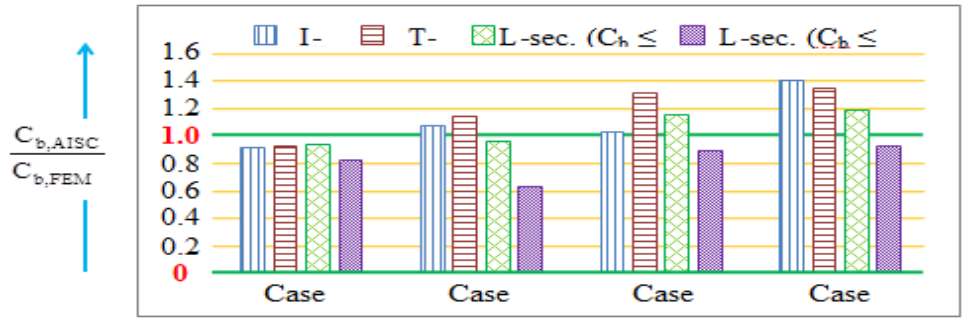

Figure-10. Response comparison between cross sections according to loading cases, β_x = + ve.

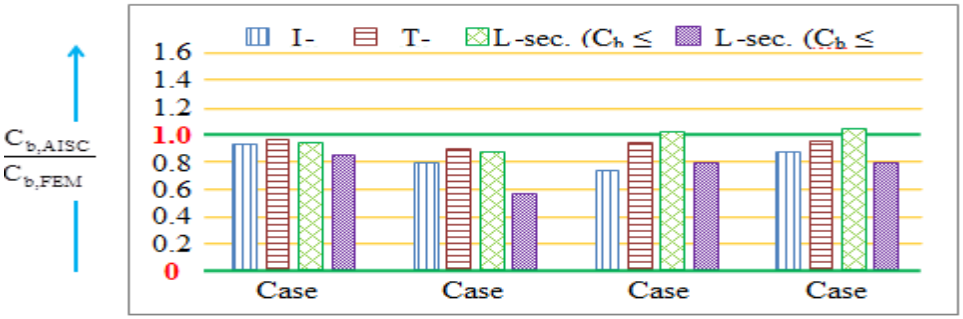

Figure-11. Response comparison between cross sections according to loading cases, β_x = - ve.

CONCLUSIONS

Lateral torsional buckling of beams is an important issue and at the same time a complex one. The finite element method offers an ideal solution for this problem. As pointed out in this paper, the traditional and classical treatment of lateral torsional buckling relies heavily on traditional methods of approximations and crude factors of safety due to the difficulties of obtaining reasonable solutions by classical mechanics methods. It was pointed out that the code even ignores the warping boundary conditions

The uncertainty and high conservatism of the correct solution render inconsistent reliability among the different components of the structure which is, in fact, contrary to the modern code philosophies of having consistent reliability indices throughout the entire structure.

As pointed out in a previous paper for the author, the FEM solution for symmetric cross sections offers a general solution that realistically and fairly accurately models all issues of lateral torsional buckling of beams. Such issues span from cross section properties and boundary conditions to loading schemes. FEM solution is a consistent and reliable solution regardless of these variations.

In this paper, it has been shown that for unsymmetric cross sections, the empirical expression becomes unreliable as it fails to capture the variation and change of sign of internal moment on LTB of beams, and hence unwarranted to provide correct and safe critical moment for the problem of LTB.

Given the above discussion, it is recommended that the codes should, at least, stop the permission of applying the empirical expression of, C_b, as is to

unsymmetric beams until a consistent expression is developed for these unsymmetric cases. The code, of course, recognizes this inconsistency of its expression when it comes to unsymmetric beams and therefore, it calls for more reliable methods to be used to obtain the critical moment.

In this paper, FEM in its simplest application of linear elements is presented as an alternative reliable solution to the fixed equations presented in the code for lateral torsional buckling of beams. It is needless to remind ourselves that at this age of availability of computers, FEM can be easily programmed and implemented in the engineering consulting practice, especially if linear elements are selected for this subject without using three-dimensional shell elements for example.

Finally, it is worth pointing out that these problems, discrepancies, and inconsistencies that appear in the, C_b, application in the case of unsymmetric cross section, do not exist in the case of symmetric cross sections. It was shown in (Armouti, 2022) that in the case of symmetric cross sections, where, β_x, is zero, the base critical moment will always be constant and is always independent of the sign of the internal moment, and hence, the, C_b, results are independent of the moment sign and distribution of the internal moment along the beam axis. Therefore, unlike the case of unsymmetric sections, the C_b, in the case of symmetric sections can still be fairly applied even if it does not provide the same level of reliability among the various cases of loading and boundary conditions.

On the contrary, the discrepancies, and inconsistencies that appear in the, C_b, application in the case of unsymmetric cross section produce a wide variation of the true critical moment where it is shown previously that unconservatism can go up to 40% of the true critical moment, whereas, the conservatism can go down up to 20% of the true critical moment. Such large variation and difference between conservatism and unconvertasim is not a good engineering practice. Such difference can be avoided by applying the simple application of FEM with linear elements as presented in this paper.

REFERENCES

Ahmad N. Z. 2021. Numerical parametric study on lateral torsional buckling of T-shaped beams containing openings. Journal of Xi'an University of Architecture & Technology, Xi'an, China. VIII(1): 570-585.

AISC. 2017. Specification for Structural Steel Buildings. American Institute of Steel Construction, Chicago, IL 60601.

Armouti N. S. 2022. Lateral Torsional Buckling of Beams Bent about Their Single Axis of Symmetry by FEM with Linear Elements. ARPN Journal of Engineering and Applied Sciences. 17(3): 344-355.

Asgarian B. and Soltani M. 2011. Lateral-Torsional Buckling of Non-Prismatic Thin-Walled Beams with Non-Symmetric Cross Sections. Proc. The 12th East Asia-Pacific Conference on Structural Engineering and Construction, Procedia Engineering. 14: 1653-1664.

Bajer M., Barnat J., Vild M, Melcher J., Karmazioniova M. and Pijak J. 2017. Different Cross-section in Lateral-torsional Buckling. Ernst & Sohn, ce/papers. 1(2 & 3): 4704-4711.

Barnat J., Bajer M., Vild M. and Melcher J. 2017. Experimental Analysis of Lateral Torsional Buckling of Beams with Selected Cross-Section Types. Proc. 18th International Conference on Rehabilitation and Reconstruction of Buildings 2016, CRRB 2016, Procedia Engineering. 14: 56-61.

Chen W. F. and Lui, E. M. 1987. Structural Stability, Theory and Implementation. Elsvier, New York.

Galambus T. V. 1968. Structural Members and Frames. Prentice-Hall, Englewood, Cliffs, New Jersey.

Hauksson H. 2014. Lateral-torsional Buckling of Steel Beams with Open Cross Section. M.Sc. Thesis, Chalmers University of Technology, Sweden.

Huebner K.H. and Thornton E.A. 1981. The Finite Element Method for Engineers. 2nd ed., John Wiley & Sons, New York.

Kirby P. A., and Nethercot, D. A. 1979. Design for Structural Stability. Constrado Monographs, Granada Publishing, UK.

Piotrowski R. and Szycchowski A. 2015. Lateral-Torsional Buckling of Beams Elastically Restrained Against Warping at Supports. Archives of Civil Engineering. LXI(4): 155-174.

Tisseur F. and Meerbergen K. 2001. The Quadratic Eigenvalue Problem. Society for Industrial and Applied Mathematics, SIAM Review. 43(2): 235-286.